CHAPTER II
LITERATURE REVIEW

2.1 Azo Dyes

2.1.1 General Remarks

The term of "azo dyes" is applied to synthetic organic colorants that are characterized by the presence of the chromophoric azo group (–N=N–). This divalent group is attached to sp^2 hybridized carbon atom on one side and to an aromatic or heterocyclic nucleus on the other. It may be linked to an unsaturated molecule of the carboxylic, heterocyclic, or aliphatic type. No natural dyes contain this chromophore. Commercially, the azo dyes are the largest and most versatile class of organic dyestuffs. There are more than 10,000 Color Index (CI) generic names assigned to commercial colorants, where approximately 4,500 are in use, and over 50% of these belong to the azo class. Synthetic dyes are derived in whole or in part from cyclic intermediates. Approximately two-thirds of the dyes are used by the textile industry to dye natural and synthetic fiber or fabrics, about one-sixth is used for coloring paper, and the rest is used chiefly in the production of organic pigments and in the dyeing of leather and plastic. Dyes are sold as pastes, powders, and liquids with concentrations varied from 6 to 100%. The concentration, form, and purity of a dye are determined largely by the use, for which it is intended.

2.1.2 Classification and Designations

The most authoritative compilation covering the constitution, properties, preparations, manufactures, and other coloring data is the publication of Color Index, which is edited jointly by the Society of Dyers and Colorists and the American Association of Textile Chemists and Colorists (AATCC). In the Color Index, a dual classification system is employed to group dyes according to area of usage and chemical constitution. Because of the ease of applications, azo dyes comprise the largest chemical class in numbers, monetary value, and tonnage produced. There are more than 2,200 chemical structures of azo dyes disclosed in the Color Index.

Nearly all dye manufactures use letters and numerals in the name of their products to define the color. Thus, B is blue; G, yellow (ge;lb in German) or green; R, red; and Y, yellow. Numerals, i.e. 2G (or GG), 3G, 4G, etc. indicate, in this case, a successively yellower or greener shade. Occasionally, suffixed letters are used to feature other properties, such as solubility, light fastness, brightness, and use on synthetic fibers.

Chemically, the azo class is subdivided according to the number of azo groups present into mono-, dis-, tris-, tetrakis-, etc. Mono- and diazo dyes are essentially equal in importance, trisazo dyes are less important, and tetrakisazo dyes, except for a few, are much less important. For this reason, substances with more than three azo linkages are generally included under the heading of polyazo dyes. Table 2.1 lists the Color Index of the azo dyes.

Table 2.1 Color Index of different azo dyes (Mary, 1991)

Chemical class	Color Index number range
Monoazo	11,000 – 19,999
Diazo	20,000 – 29,999
Trisazo	30,000 – 34,999
Polyazo	35,000 – 36,999

2.2 Semiconductor

A semiconductor is a material with an electrical conductivity that is intermediate between that of an insulator and a conductor. Like other solids, semiconductor materials have electronic band structure determined by the crystal properties of the material. A semiconductor used as photocatalyst should be an oxide or sulfide of metals, such as TiO_2, CdS, and ZnO. The actual energy distribution among electrons is described by the Fermi level and temperature of the electrons. At absolute zero temperature, all of the electrons have energy below the Fermi energy, but at non-zero temperature, the energy levels are randomized, and some electrons have energy above the Fermi level.

Among the bands filled with electrons, the one with the highest energy level is referred to as the valence band, and the band outside of this is referred to as the conduction band. The energy width of the forbidden band between the valence band and the conduction band is referred to as the band gap. The overall structure of band gap energy is shown in Figure 2.1.

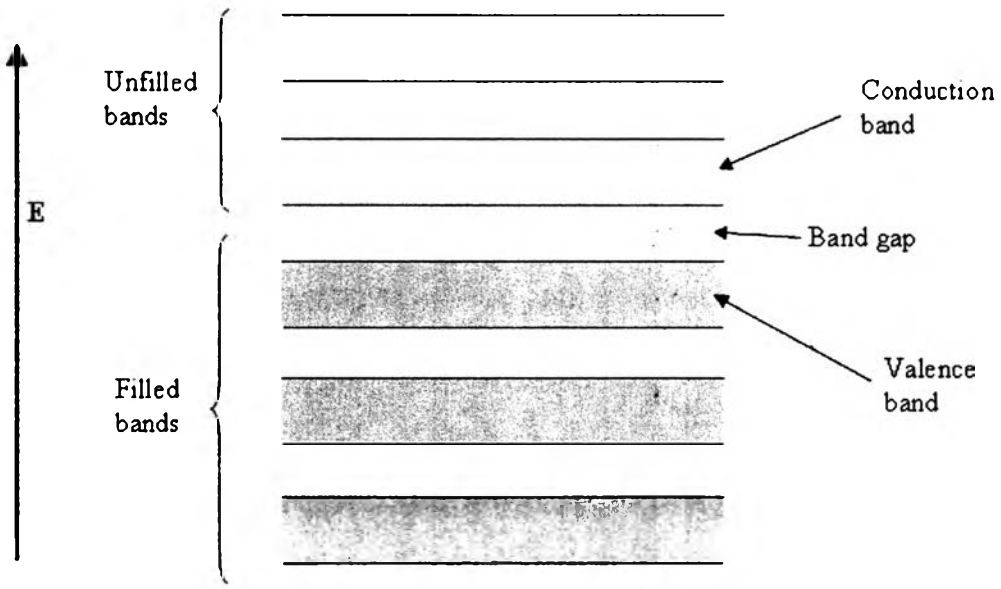

Figure 2.1 The structure of band gap energy.

The band gap can be considered as a wall that electrons must jump over in order to become free. The amount of energy required to jump over the wall is referred to as the band gap energy (E_g, eV). Only electrons that jump over the wall and enter the conduction band (CB, which are referred to as conduction band electrons) can move around freely. When light is illuminated at appropriate wavelengths with energy equal or more than band gap energy, valence band (VB) electrons can move up to the conduction band (CB). At the same time, as many positive holes as the number of electrons that have jumped to the conduction band (CB) are created. The valence band (VB), conduction band (CB), band gap, and band gap wavelength of some common semiconductors are shown in Table 2.2.

Table 2.2 The band gap positions of some common semiconductor photocatalysts (Robertson, 1996; Vali, 2007; and Moreira *et al.*, 2009)

Semiconductor	Valence band (eV)	Conduction band (eV)	Band gap (eV)	Band gap wavelength (nm)
TiO_2	+3.1	-0.1	3.2	387
SnO_2	+4.1	+0.3	3.8	326
$SrTiO_3$	+3.1	-0.1	3.2	387
$SrZrO_3$	+4.3	-1.3	5.6	221
ZnO	+3.0	-0.2	3.2	387
ZnS	+1.4	-2.3	3.7	335
WO_3	+3.0	+0.2	2.8	443
CdS	+2.1	-0.4	2.5	496
CdSe	+1.6	-0.1	1.7	729
GaAs	+1.0	-0.4	1.4	886
GaP	+1.3	-1.0	2.3	539

2.3 Photocatalysts

Powders with semiconductor characteristics have been widely employed in photocatalytic systems because they are capable of generating charge carriers by absorbing photon energies. The separation effectiveness of the photo-induced charge carriers is an important factor in determining the photocatalytic activity of the powders. One promising photocatalyst is perovskite-related material. Perovskite-related materials are represented by the general formula of ABO_3 (A = rare earth and alkali element with or without its partial substitution by alkaline earth element, and B = transition element, such as Co, Mn, Ti, Ta, Ni, Fe, etc., with or without its partial substitution) (Hu *et al.*, 2007).

Strontium titanate ($SrTiO_3$) is a well-known cubic-perovskite paraelectric oxide with a large dielectric constant, which has attracted a great deal of attention due to its excellent dielectric, photoelectric, optical, and catalytic properties. $SrTiO_3$

is also considered to be useful for photocatalytic decomposition of water in place of conventional photocatalysts, such as TiO_2, because its CB level provides a higher photopotential than TiO_2 and facilitates hydrogen formation (Subramanian *et al.*, 2006). However, pure $SrTiO_3$ without cocatalysts showed very low photocatalytic activity. Therefore, the modification of $SrTiO_3$ is necessary to obtain active photocatalysts for the photocatalytic degradation of dyes from wastewater. For example, Ag, Au, Cr, Pt, Pd, and Zr have been incorporated into $SrTiO_3$. The photocatalytic activity enhancement by Ag doping on $SrTiO_3$ was reported by Subramanian *et al.* (2006). $SrTiO_3$ doped with Cr^{3+} led to an introduction of isolated energy levels within its band gap, so photon can be absorbed at two levels, the band gap and the sub-band gap, where the latter led to light absorption in the visible region (Ashokkumar, 1998).

Puangpetch *et al.* (2008) investigated the synthesis and photocatalytic activity in Methyl Orange degradation of mesoporous-assembled $SrTiO_3$ nanocrystals prepared by a sol-gel method with the aid of structure-directing surfactant. The results showed that the $SrTiO_3$ nanocrystals were successfully synthesized by using strontium nitrate ($Sr(NO_3)_2$) and tetraisopropyl orthotitanate (TIPT) as precursors. Anhydrous ethanol (EtOH), ethylene glycol (EG), or EtOH/EG was selected as a solvent, while laurylamine hydrochloride (LAHC), cetyltrimethylammonium bromide (CTAB), or cetyltrimethylammoniumchloride (CTAC) was used as a structure-directing surfactant. The effects of the MO photodegradation by the $SrTiO_3$, such as crystallinity, specific surface area, and pore characteristic, were investigated. The mesoporous-assembled structure with a high pore uniformity of $SrTiO_3$ plays the most important role affecting the photocatalytic activity of the $SrTiO_3$ photocatalyst. The $SrTiO_3$ with the mesoporous-assembled structure and narrow pore size distribution synthesized at a calcination temperature of 700°C, a heating rate of 1°C min^{-1}, a LAHC-to-TIPT molar ratio of 0.25:1, and using an EtOH solvent provided the highest photocatalytic degradation activity, which was much higher than that of the non-mesoporous-structured commercial $SrTiO_3$.

Chen *et al.* (2008) investigated the synthesis of Zr-doped $SrTiO_3$ prepared by a sol-gel method and its photocatalytic degradation for Methylene Blue. Their results showed that the 8% of Zr content doped on $SrTiO_3$ provided the highest

photocatalytic degradation rate due to free zirconium ions that cannot reach $SrTiO_3$ crystal and induced $SrTiO_3$ to absorb light.

Strontium zirconate ($SrZrO_3$) also belongs to the perovskite family and has an orthorhombic structure at room temperature with space group *Pbnm*. However, more recent studies on high-temperature investigation have shown that $SrZrO_3$ has the following sequence of phase transitions. First, orthorhombic (*Pnma*) was transformed to orthorhombic (*Cmcm*) at 973 K, then to tetragonal (*I4/mcm*) at 1,103 K, and finally the structure was found to be the ideal cubic perovskite (*Pm3m*) at 1,400 K (Feng *et al.*, 2001). This compound has a high melting temperature of about 2,923 K, so it is cubic in a wide range of temperature where most of its useful applications take place. Perovskite oxides are important materials for various functional devices. $SrZrO_3$-based perovskite oxides have been studied for their high-temperature protonic conductivity, which makes them potential candidates for electrolytes in some novel electrochemical devices, such as solid oxide fuel cells and hydrogen sensors. Besides, $SrZrO_3$ has many characteristics, which are suitable for high voltage and high reliability capacitor applications. It also has high dielectric constant, high breakdown strength, and low leakage current density. It also has a large optical gap of 5.6 eV (Vali, 2007)

Cavalcante *et al.* (2007) studied the synthesis, characterizations, and optical absorption behavior of $SrZrO_3$ powders obtained by a chemical method. The results showed that the $SrZrO_3$ powders free of secondary phases and with orthorhombic structure were obtained from the polymeric precursor method. Rietveld analysis confirmed the orthorhombic phase with space group *Pbmn*. Less variations in the lattice parameters were observed in crystalline $SrZrO_3$ powders heat-treated at 1,123 and 1,223 K for 2 h. XRD patterns suggested that the crystallization of $SrZrO_3$ powders started at 848 K while Raman analysis revealed that the $SrZrO_3$ powders treated at 748 K presented a beginning of structural order at short range. UV-visible spectra showed the presence of localized levels in the band gap of disordered $SrZrO_3$ powders, and these levels were reduced with the increase of structural order, as shown in Table 2.3.

Table 2.3 Data obtained from UV-visible spectra for $SrZrO_3$ obtained by different methods Cavalcante *et al.* (2007)

Method	Temperature (K)	Time	Optical gap (eV)
PPM	748	2 h	4.49
PPM	773	2 h	4.91
PPM	973	2 h	4.96
PPM	1,123	2 h	5.02
PPM	1,223	2 h	5.04
PPM	1,423	2 h	5.11
PPM	1,523	2 h	5.22
FZ	-	-	5.41
SGC	973	1 h	5.2
PLD	673	5 min	5.7
SG	773	5 min	4.63
MOD	873	-	5.5

PPM = polymeric precursor method; FZ = floating zone; SGC = sol-gel combustion; PLD = pulsed laser deposition; SG = sol-gel, and MOD = metallo-organic decomposition.

Wong *et al.* (2001) studied the crystal structures and phase transitions in the $SrTi_xZr_{1-x}O_3$ solid solution. The results showed that superlattice reflections in the neutron diffraction patterns were proved to be the most reliable indicators of lower symmetry structures. At room temperature, the structures were orthorhombic *Pbnm* in the range of $0 \leq x \leq 0.4$, tetragonal *I4/mcm* in the range $0.4 \leq x \leq 0.95$, and cubic *Pm3m* for $0.95 \leq x \leq 1$. Additionally, they studied the two room-temperature tetragonal samples ($x = 0.5, 0.75$) by using neutron diffraction methods for additional high variable temperature. The tetragonal-to-cubic phase transition for $SrTi_{0.5}Zr_{0.5}O_3$ occurred between 948 and 998 K, whereas that for $SrTi_{0.75}Zr_{0.25}O_3$ occurred between 573 and 623 K.

2.4 Nano-Photocatalysts

2.4.1 General Remarks

Nanocrystalline photocatalysts are ultra-small semiconductor particles, which are few nanometers in size. During the past decade, the photochemistry of nanosized semiconductor particles has been one of the fastest growing research areas in physical chemistry. The interest in these small semiconductor particles originates from their unique photophysical and photocatalytic properties. Several review articles have been published concerning the photophysical properties of nanocrystalline semiconductors. Such studies have demonstrated that some properties of nanocrystalline semiconductor particles are in fact different from those of bulk materials.

Nanosized particles possess properties with falling into the region of transition between the molecular and bulk phases. In the bulk material, the electron excited by light absorption funds a high density of states in the conduction band, where it can exist with different kinetics energies. In the case of nanoparticles, however the particle size is the same as or smaller than the size of the first excited state. Thus, the electrons and holes generated upon illumination cannot suit into such a particle, unless they assume a state of higher kinetics energy.

Hence, as the size of the semiconductor particle is reduced below a critical diameter, the spatial confinement of the charge carriers within a potential well, like ''a particle in a box'', causes them to mechanically behave quantum. In solid state terminology, this means that the bands split into discrete electronic states (quantized levels) in the valence and conduction bands, and the nanoparticle progressively behaves similar to a giant atom. Nanosized semiconductor particles, which exhibit size-dependent optical and electronic properties, are called quantized particles or quantum dots (Kamat, 1995).

2.4.2 Activity of Nano-Photocatalysts

One of the main advantages of the application of nanosized particles is the increase in the band gap energy with decreasing particle size. As the size of a semiconductor particle falls below the critical radius, the charge carriers begin to

behave mechanically quantum, and the charge confinement leads to a series of discrete electronic states. As a result, there is an increase in the effective band gap and a shift of the band edges. Thus by varying the size of the semiconductor particles, it is possible to enhance the redox potential of the valence band holes and the conduction band electrons.

However, the solvent reorganizational free energy for charge transfer to a substrate remains unchanged. The increasing driving force and the unchanged solvent reorganizational free energy are expected to lead to an increase in the rate constants for charge transfer at the surface. The use of nanosized semiconductor particles may result in increased photocatalytic activity for systems, in which the rate-limiting step is interfacial charge transfer. Hence, nanosized semiconductor particles can possess enhanced photoredox chemistry with reduction reactions, which might not otherwise proceed in bulk materials, being able to occur readily using sufficiently small particles. Another factor, which could be advantageous, is the fact that the fraction of atoms that are located at the surface of a nanoparticle is very large. Nanosized particles also have high surface area to volume ratios, which further enhances their catalytic activity. One disadvantage of nanosized particles is the need for light with a shorter wavelength for photocatalyst activation. Thus, a smaller percentage of a polychromatic light source will be useful for photocatalysis.

2.5 Photocatalytic Degradation of Dyes

2.5.1 Photocatalytic Oxidation

It is well established that conduction band electrons (e^-) and valence band holes (h^+) are generated when aqueous photocatalyst suspension is irradiated with light energy greater than its band gap energy. The photogenerated electrons can reduce the dye or react with electron acceptors, such as O_2 adsorbed on the photocatalyst surface or dissolved in water, reducing it to superoxide radical anion $O_2^{\bullet -}$. The photogenerated holes can oxidize the organic molecule to form R^+ or react with OH^- or H_2O, oxidizing them into $OH^\bullet$ radicals. Together with other highly oxidant species (peroxide radicals), they are reported to be responsible for the heterogeneous photocatalytic degradation of organic substrates as dyes. According to

this, the relevant reactions at the semiconductor surface causing the degradation of dyes can be expressed as follows:

$$\text{photocatalyst} + h\nu(\text{UV}) \rightarrow \text{photocatalyst}(e_{CB}^- + h_{VB}^+) \quad (1)$$

$$\text{photocatalyst}(h_{VB}^+) + H_2O \rightarrow \text{photocatalyst} + H^+ + OH^\bullet \quad (2)$$

$$\text{photocatalyst}(h_{VB}^+) + OH^- \rightarrow \text{photocatalyst} + OH^\bullet \quad (3)$$

$$\text{photocatalyst}(e_{CB}^-) + O_2 \rightarrow \text{photocatalyst} + O_2^{\bullet-} \quad (4)$$

$$O_2^{\bullet-} + H^+ \rightarrow HO_2^\bullet \quad (5)$$

$$\text{Dye} + OH^\bullet,\ HO_2^\bullet, O_2^{\bullet-} \rightarrow \text{degradation products} \quad (6)$$

$$\text{Dye} + h_{VB}^+ \rightarrow \text{oxidation products} \quad (7)$$

$$\text{Dye} + e_{CB}^- \rightarrow \text{reduction products} \quad (8)$$

The resulting $OH^\bullet$ radical, being a very strong oxidizing agent (standard redox potential of +2.8 V), as well as $HO_2^\bullet$ and $O_2^{\bullet-}$, can oxidize most of azo dyes to the mineral end products. Substrates not reactive toward hydroxyl radicals are degraded employing photocatalysis with rates of decay highly influenced by the semiconductor valence band edge position. The role of reductive pathways (Equation (8)) in heterogeneous photocatalysis has been envisaged also in the degradation of several dyes but in a minor extent than oxidation.

2.5.2 Photosensitized Oxidation

The mechanism of photosensitized oxidation (called also photoassisted degradation) by visible radiation ($\lambda > 420$ nm) is different from the pathway implicated under UV light radiation. In the former case, the mechanism suggests that excitation of the adsorbed dye takes place by visible light to appropriate singlet or triplet states, subsequently followed by electron injection from the excited dye molecule into the conduction band of the photocatalyst particles, whereas the dye is converted to the cationic dye radicals ($Dye^{\bullet+}$) that undergoes degradation to yield products as follows:

$$\text{Dye} + h\nu(\text{visible}) \rightarrow {}^1\text{Dye}^* \text{ or } {}^3\text{Dye}^* \quad (9)$$

$${}^1\text{Dye}^* \text{ or } {}^3\text{Dye}^* + \text{photocatalyst} \rightarrow \text{Dye}^{\bullet+} + \text{photocatalyst}(e_{CB}^-) \quad (10)$$

$$\text{photocatalyst}(e_{CB}^-) + O_2 \rightarrow O_2^{\bullet-} + \text{photocatalyst} \quad (11)$$

$$\text{Dye}^{\bullet+} \rightarrow \text{degradation product} \quad (12)$$

The cationic dye radicals readily react with hydroxyl ions undergoing oxidation via Equations (13) and (14) or interact effectively with $O_2^{\bullet-}$, $HO_2^{\bullet}$, or $HO^{\bullet-}$ species to generate intermediates that ultimately lead to CO_2 (Equations (15) – (19)).

$$Dye^{\bullet+} + OH^- \rightarrow Dye + HO^{\bullet} \quad (13)$$

$$Dye + 2HO^{\bullet} \rightarrow H_2O + \text{oxidation products} \quad (14)$$

$$O_2^{\bullet-} + H^+ \rightarrow HO_2^{\bullet} \quad (15)$$

$$HO_2^{\bullet} + H^+ + \text{photocatalyst}(e_{CB}^-) \rightarrow H_2O_2 + \text{photocatalyst} \quad (16)$$

$$H_2O_2 + \text{photocatalyst}(e_{CB}^-) \rightarrow HO^{\bullet} + HO^- + \text{photocatalyst} \quad (17)$$

$$Dye^{\bullet+} + O_2^{\bullet-} \rightarrow DO_2 \rightarrow \text{degradation products} \quad (18)$$

$$Dye^{\bullet+} + HO_2^{\bullet}(\text{or } HO^{\bullet}) \rightarrow \text{degradation products} \quad (19)$$

When using sunlight or simulated sunlight (laboratory experiments), it is suggested that both photooxidation and photosensitizing mechanism occurs during the irradiation, and both photocatalyst and the light source are necessary for the reaction to occur. In the photocatalytic oxidation, photocatalyst has to be irradiated and excited in a near-UV energy to induce charge separation. On the other hand, dyes rather than photocatalyst can be excited by visible light followed by electron injection into photocatalyst conduction band, which leads to photosensitized oxidation. It is difficult to conclude whether the photocatalytic oxidation is superior to the photosensitizing oxidation mechanism, but the photosensitizing mechanism will help improve the overall efficiency and make the photobleaching of dyes using solar light more feasible.

2.6 Metal-Loaded $SrTiO_3$ for Photocatalytic Degradation Improvement

The strontium titanate ($SrTiO_3$) has been widely investigated for the degradation of various organic contaminants, such as dyes and other organic compounds, to solve environmental problems and for water splitting to produce clean energy. However, the biggest obstacle that prevents its application to industrial or domestic wastewater on a large scale is that the separation of photocatalyst from suspension after the reaction is difficult, and the suspended particles tend to aggregate at high concentrations. Attempts to increase the photocatalytic efficiency of strontium titanate have been made by doping other coupled semiconductor

photocatalysts and by coating and doping with transition metals and noble metals. Therefore, the charge separation in the photocarrier generation is enhanced, and the energy needed for photoexcitation is reduced, both of which allow modified titanium dioxide to absorb light efficiently and to initiate the reaction rapidly (Yang *et al.*, 2004).

Chang *et al.* (2005) studied the photocatalytic degradation of Methylene Blue (MB) under visible light irradiation using chromium-doped $SrTiO_3$ photocatalyst synthesized by a polymeric precursor method. The results showed that the photocatalytic MB degradation of the $SrTi_{(1-x)}Cr_xO_3$ with x = 0.02 was much higher than the pure $SrTiO_3$ because the spectra of $SrTi_{(1-x)}Cr_xO_3$ with x = 0.02 exhibited obvious absorption in visible light region (red-shift). The charge-transfer transition between Cr-ion 3d electrons and conduction band may explain the appearance of the red-shift.

Subramanian *et al.* (2006) studied the photocatalytic degradation of Victoria Blue dye by using strontium titanate ($SrTiO_3$) perovskite films unloaded and loaded with some metals (Ag, Pt, Au) prepared by a modified Pachini process. The results showed that the Ag and Pt loadings provided a better photocatalytic activity than the plain $SrTiO_3$. These may be possibly because the metals can reduce the recombination of charges by acting as an electron sink on the $SrTiO_3$ surface. However, the highest photocatalytic degradation of Victoria Blue under UV-visible-light illumination was observed at the 1.0 wt.% Ag-loaded $SrTiO_3$ photocatalyst.

Jia *et al.* (2010) investigated the photocatalytic degradation of Malachite Green (MG) under visible light irradiation using Ni,La-codoped $SrTiO_3$ photocatalysts synthesized by a sol-gel method compared with the commercial Degussa P25 TiO_2 photocatalyst. The MG degradation rate of all synthesized photocatalysts exhibited a much higher activity than the commercial photocatalyst. The promising photocatalyst was 1.0% Ni,La-codoped $SrTiO_3$ exhibiting the highest photocatalytic activity. The high activity was a result of the best combination of many properties, such as the intensive visible light response, the large surface area and pore volume, and the high initial adsorption rate of substrate.

2.7 Factors Influencing Photocatalytic Degradation of Dyes

2.7.1 Effect of Initial Dye Concentration

Yao *et al.* (2004) studied the degradation of Methyl Orange (MO) by perovskite bismuth titanate, $Bi_4Ti_3O_{12}$, prepared by using a chemical solution decomposition (CSD) method. The results showed that with different MO concentrations varied from 5 to 20 mg/l, the degradation efficiency decreased with increasing MO concentration. The strong decrease in the observed rate constants with the increase in initial dye concentration was attributed to the significant absorption of light by the substrate in the same wavelength range of photocatalyst excitation. For increasing the initial MO concentration, the photon flow reaching the photocatalyst particles decreased due to the fact that with increasing aliquots, photons are absorbed by the MO molecules present in the solution and/or on the photocatalyst surface. Moreover, this dependence can also be related to the formation of several layers of adsorbed dye on the photocatalyst surface, which is higher at higher dye concentrations. The large amount of adsorbed dye inhibits the reaction of dye molecules with photogenerated holes or hydroxyl radicals because of the increased distance between reactants and photocatalysts.

2.7.2 Effect of Solution pH

The heterogeneous photocatalysis has been found to be pH dependent. Yao *et al.* (2004) also studied the effect of solution pH on the MO degradation by the bismuth titanate, $Bi_4Ti_3O_{12}$. The results showed that with different initial pH values (1.22, 2.43, 5.18, 7.13, 10.2, and 12.7), the reaction rate increased at acidic pH, but decreased at alkaline pH. The effect of pH on the degradation of the pollutants is variable and controversial. The increase in degradation rate at acidic pH was explained on the basis that at low pH, HO_2 radicals will form, and this will compensate for the effect of decreasing hydroxyl ion concentration. The decrease in degradation rate at alkaline pH is assumed to be due to the anions and the highly negative charged oxide surface, and the degradation would, thus, depend on diffusion of surface-generated $OH^{\bullet}$ towards the inside layer to the low concentration of MO anion, a slower process than direct charge transfer.

2.7.3 Effect of Light Intensity and Irradiation Time

Ollis *et al.* (1991) reviewed the studies reported for the effect of light intensity on the kinetics of the photocatalysis process and stated that (i) at low light intensities (0-20 mW/cm^2), the rate would increase linearly with increasing light intensity (first order), (ii) at intermediate light intensities beyond a certain value (approximately 25 mW/cm^2), the rate would depend on the square root of the light intensity (half order), and (iii) at high light intensities, the rate is independent of light intensity. This is likely because at low light intensity, reactions involving electron-hole formation are predominant, and electron-hole recombination is negligible. However, at increased light intensity, electron-hole pair separation competes with recombination, thereby causing lower effect on the reaction rate. It is evident that the percentage of degradation increases with an increase in irradiation time. The reaction rate decreases with irradiation time since it follows apparent first-order kinetics, and additionally, a competition for degradation may occur between the reactant and the intermediate products. The slow kinetics of dye degradation after a certain time is due to:

- The difficulty in converting the N-atoms of dye into oxidized nitrogen compounds
- The slow reaction of short chain aliphatics with $OH^{\bullet}$ radicals
- The short life-time of photocatalyst

because of active site deactivation by strong by-product adsorption (Konstantinou and Albanis., 2004).

2.7.4 Effect of Calcination Temperature of Photocatalyst

Puangpetch *et al.* (2008) studied the effect of calcination temperature of the mesoporous-assembled $SrTiO_3$ photocatalyst (600, 650, 700, and 750°C) on the MO degradation. The results showed that the with the mesoporous-assembled structure and narrow pore size distribution synthesized at the calcination temperature of 700°C provided the highest photocatalytic degradation activity.

Zhang *et al.* (2004) studied the photocatalytic activity of ZnO-SnO_2 mixed oxides for the MO degradation, and the effect of heat treatment at different

calcination temperatures (300, 350, 400, 450, 500, 600, 700, 800, and 900°C) was investigated. The results showed that the degradation rate increased with increasing calcination temperature except for 300°C because of the partial formation of crystallite oxides. With increasing calcination temperature, the size of crystallite oxides increased, contributing to the increase in photocatalytic activity. However, at temperatures higher than 700°C, the photocatalyst exhibited poor activity because of the negative effect of the coupled oxides.

2.7.5 Effect of Calcination Time of Photocatalyst

Yao *et al.* (2004) also studied the effect of calcination time on the photocatalytic activity of the $Bi_4Ti_3O_{12}$ photocatalyst calcined at 600°C. The results showed that at 1 min calcination time for thin film photocatalyst, the highest MO degradation was obtained. While the rate constant increased with increasing calcination temperature, but at calcination time of 5 min, the rate constant reached the highest value because at higher calcination time of 10 min, the sintering of photocatalyst material occurred.

2.8 Porous Materials

The classification of pores according to size has been under discussion for many years, but in the past, the terms ''micropore'' and ''macropore'' have been applied in different ways by physical chemists and some other scientists. In an attempt to clarify this situation, the limits of size of the different categories of pores included in Table 2.4 have been proposed by the International Union of Pure and Applied Chemistry (IUPAC) (Ishizaki *et al.*, 1988 and Rouquerol *et al.*, 1999). As indicated, the ''pore size'' is generally specified as the ''pore width'', i.e. the available distance between the two opposite walls. Obviously, pore size has a precise meaning when the geometrical shape is well defined. Nevertheless, for most purposes, the limiting size is that of the smallest dimension, and this is generally taken to represent the effective pore size. Micropores and mesopores are especially important in the context of adsorption.

Table 2.4 Definitions about porous solids

Term	Definition
Porous solid	Solid with cavities or channels which are deeper than they are wide
Micropore	Pore of internal width less than 2 nm
Mesopore	Pore of internal width between 2 and 50 nm
Macropore	Pore of internal width greater than 50 nm
Pore size	Pore width (diameter of cylindrical pore or distance between opposite walls of slit)
Pore volume	Volume of pores determined by stated method
Surface area	Extent of total surface area determined by given method under stated conditions

According to the IUPAC classification, porous materials are regularly organized into three categories on a basis of predominant pore size as follows:

- Microporous materials (pore size < 2 nm) include amorphous silica and inorganic gel to crystalline materials, such as zeolites, aluminophosphates, gallophosphates, and related materials.
- Mesoporous materials (2 nm ≤ pore size ≤ 50 nm) include the M41S family (e.g. MCM-41, MCM-48, MCM-50, and etc.) and other non-silica materials synthesized via intercalation of layered materials, such as double hydroxides, metal (titanium, zirconium) phosphates, and clays.
- Macroporous materials (pore size > 50 nm) include glass-related materials, aerogels, and xerogels.

Nowadays, micro- and mesoporous materials are generally called ''nanoporous materials''. Particularly, mesoporous materials are remarkably very suitable for catalysis applications, whereas the pores of microporous materials may become easily plugged during catalyst preparation if high loading is used.

2.9 Sol-Gel Process

The sol-gel process has been intensively studied because it is so effective to prepare nano-sized mesoporous materials (Sreethawong *et al.*, 2005). Because the perovskite oxides can be deactivated due to sintering or crystal growth during their continuous use in high temperature processes, and the photocatalytic performance of the perovskite oxides is well-known to depend on their specific surface area, a sol-gel method presents some particular advantages through a low-temperature process, avoiding contamination of the materials. It also yields better stoichiometric control and the possibility of grain-size and grain-shape control. This technique does not require complicated instruments, such as in chemical vapor deposition method. It provides a simple and easy means for synthesizing nano-sized particles, which is essential for nano-photocatalysts (Wu and Chen, 2004). It involves the formation of metal-oxo-polymer network from molecular precursors, such as metal alkoxides, and subsequent polycondensation, as follows:

$$\text{M-OR} + \text{H}_2\text{O} \rightarrow \text{M-OH} + \text{ROH} \quad (20)$$

$$\text{M-OH} + \text{M-OR} \rightarrow \text{M-O-M} + \text{R-OH} \quad (21)$$

$$\text{M-OH} + \text{M-OH} \rightarrow \text{M-O-M} + \text{H}_2\text{O} \quad (22)$$

where M = Si, Ti, Zr, Al, and R = alkyl group. All stages, including the formation of colloid particles to form gel network, drying of wet gel, and calcination stage, can all lead to grain growth and formation of agglomerates. Hence, to carefully control the process is very essential in preparing high performance and high reproducibility powders. The relative rates of hydrolysis and polycondensation strongly influence the structure and properties of the resulting metal oxides. Typically, sol-gel-derived precipitates are amorphous in nature, requiring further heat treatment to induce crystallization. The calcination process frequently gives rise to particle agglomeration and grain growth, and may induce phase transformation (Wang and Ying, 1999). Thus, a surfactant is used to prevent agglomeration of the particles. The $BaTiO_3$ nanoparticles synthesized by a sol-gel process (Yu *et al.*, 2008), however, are easy to agglomerate. This can be avoided by the application of the surfactant, i.e. oleic acid, as cheap and innoxious surfactant, thus preventing the agglomeration of particles. The sol-gel process by the addition of surfactant can help enforce size

controllability and prepare well-dispersed powders. The ideal model of forming the $BaTiO_3$ nanoparticles is shown in Figure 2.2.

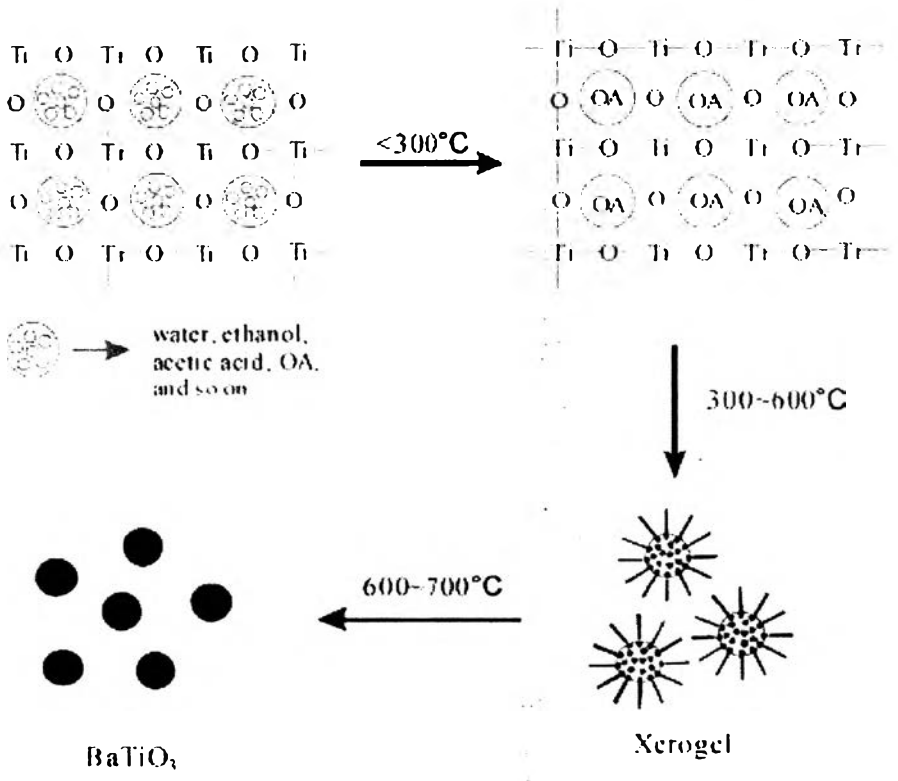

Figure 2.2 A schematic of forming the $BaTiO_3$ nanoparticles (Yu *et al.*, 2008).

The process can be divided to three steps. Firstly, oleic acid (OA) enchases in the 3D network structure of -Ti-O-Ti- when the temperature is lower than 300°C. Secondly, between 300 and 600°C, a number of "microcapsules" of $BaTiO_3$ precursors coated by OA are formed. The carboxyl of OA is towards the inside and hydrophobic -R group towards the outside. Excessive OA as solution will allow the system to form "microcapsules". Finally, when the temperature is higher than 600°C, OA decomposes, and the walls of "microcapsules" are destroyed. Although this happens, the shape of $BaTiO_3$ precursor is preserved, thus producing better-dispersed $BaTiO_3$ nanoparticles.

Factors affecting the sol-gel process include the reactivity of metal alkoxides, pH of the reaction medium, water-to-alkoxide ratio, reaction temperature, and nature of solvent and additive. The water-to-alkoxide ratio governs the sol-gel chemistry

and the structural characteristics of the hydrolyzed gel. High water-to-alkoxide ratio in the reaction medium ensures a more complete hydrolysis of alkoxides, favoring nucleation versus particle growth. In addition, an increase in water-to-alkoxide ratio leads to reducing the crystallite size of the calcined sample. An alternative approach to control the sol-gel reaction rates involves the use of acid or base catalyst. It was reported that for a system with a water-to-alkoxide ratio of 165, the addition of HCl resulted in the reduction of the crystallite size from 20 to 14 nm for the samples calcined at 450°C. Besides, a finer grain size and a narrower pore size distribution with a smaller average pore diameter were also attained for the sample synthesized with HCl (Wang and Ying, 1999). The size of alkoxide group in alkoxides also plays an important role in controlling the particle size. The titanium alkoxide containing bulky groups, such as titanium amiloxide, reduces the hydrolysis rate, which is advantageous for the preparation of fine colloidal particles (Murakami *et al.*, 1999).